Molecular Therapy
Original Article

Neonatal Systemic AAV-Mediated Gene Delivery of GDF11 Inhibits Skeletal Muscle Growth

Quan Jin,[1] Chunping Qiao,[1] Jianbin Li,[1] Juan Li,[1] and Xiao Xiao[1]

[1]Division of Pharmacoengineering and Molecular Pharmaceutics, Eshelman School of Pharmacy, University of North Carolina at Chapel Hill, Chapel Hill, NC 27599, USA

Growth and differentiation factor 11 (GDF11; BMP11) is a circulating cytokine in the transforming growth factor beta (TGF-β) superfamily. Treatment with recombinant GDF11 (rGDF11) protein has previously been shown to reverse skeletal muscle dysfunction in aged mice. However, the actions of GDF11 in skeletal muscle are still not fully understood. Because GDF11 activates the TGF-β-SMAD2/3 pathway, we hypothesized that GDF11 overexpression would inhibit skeletal muscle growth. To test this hypothesis, we generated recombinant adeno-associated virus serotype 9 (AAV9) vectors harboring the gene for either human GDF11 (AAV9-GDF11) or human IgG1 Fc-fused GDF11 propeptide (AAV9-GDF11Pro-Fc-1) to study the effects of GDF11 overexpression or blockade on skeletal muscle growth and function *in vivo*. After intravenous administration of AAV9-GDF11 into neonatal C57BL/6J mice, we observed sustained limb muscle growth inhibition along with reductions in forelimb grip strength and treadmill running endurance at 16 weeks. Conversely, treatment with AAV9-GDF11Pro-Fc-1 led to increased limb muscle mass and forelimb grip strength after 28 weeks, although a difference in the total body mass/muscle mass ratio was not observed between treatment and control groups. In sum, our results suggest GDF11 overexpression has an inhibitory effect on skeletal muscle growth.

INTRODUCTION

The more-than-30 members of the transforming growth factor β (TGF-β) superfamily have critical roles in cell development, differentiation, and proliferation in embryonic and adult tissues. TGF-β signaling has essential functions in the regulation of muscle growth and homeostasis, and pharmacologic modulation of TGF-β signaling has been actively studied for the treatment of muscular diseases.[1–3] The growth and differentiation factor 11 (GDF11; also known as BMP11) is a secreted protein belonging to the TGF-β superfamily. GDF11 is translated as a precursor protein that is proteolytically processed to an N-terminal propeptide and a C-terminal disulfide-linked homodimer. After initial cleavage, the N-terminal GDF11 propeptide remains associated with the C-terminal GDF11 homodimer in an inactive latent complex. An additional proteolysis step cleaves the GDF11 propeptide, leading to the release of the active GDF11 homodimer. Studies *in vitro* and *in vivo* have shown that this active GDF11 homodimer is inhibited in the presence of the full-length N-terminal GDF11 propeptide.[4,5] GDF11 has previously been identified as a critical factor for axial patterning, neuronal development, and kidney and pancreas organogenesis in the developing embryo.[6–9] In the olfactory epithelium, GDF11 has been shown to play a role in the regulation of neurogenesis.[10] However, GDF11 effects in skeletal muscle remain poorly understood.

Recently, GDF11 has been recognized as a potential anti-aging factor after its identification from novel mouse heterochronic parabiosis experiments.[11] Circulating GDF11 was found to decline with age, and restoration of GDF11 levels by recombinant GDF11 (rGDF11) injections in aged mice restored muscle integrity, reversed pathologic cardiac hypertrophy, and induced vascular remodeling and neurogenesis in the brain.[11–13] In its active domain, GDF11 possesses 90% homology to the TGF-β superfamily member myostatin (also known as GDF8).[14] Both GDF11 and myostatin signal via a heterodimeric complex consisting of a serine-threonine kinase activin receptor type II (ActRII) and type I activin receptor-like kinase 4/5 (ALK4/5). Ligand binding to ActRII triggers ALK4/5 phosphorylation, which mediates phosphorylation of transcription factors SMAD2/3. Activated SMAD2/3 forms a complex with SMAD4 and translocates to the nucleus, where it may elicit changes in gene expression.[15,16] ActRII activation is known to inhibit myogenesis, and blockade of ActRII or its ligands results in skeletal muscle hypertrophy.[16] The close similarity between GDF11 and myostatin, which is a known negative regulator of myogenesis, raises questions about the true role of GDF11 in the context of aging skeletal muscle, although the possibility that GDF11 mediates its anti-aging effects via alternative mechanisms cannot be ruled out. Since the initial discovery of GDF11 as an anti-aging factor, conflicting studies have emerged.[17–20] Questions regarding the validity of GDF11 detection methods and significance of pathological cardiac hypertrophy in aged mice have further complicated the field.[21,22]

As described in several reports, inconsistencies in reagents may be partly responsible for the discrepancy in observations with GDF11 studies.[21–23] Earlier GDF11 studies primarily utilized rGDF11 synthesized in bacterial protein production systems. Recombinant protein administration is subject to variability in dosing, activity, and

Received 2 August 2017; accepted 16 January 2018;
https://doi.org/10.1016/j.ymthe.2018.01.016.

Correspondence: Xiao Xiao, PhD, Division of Pharmacoengineering and Molecular Pharmaceutics, Eshelman School of Pharmacy, University of North Carolina at Chapel Hill, Chapel Hill, NC, USA.
E-mail: xxiao@email.unc.edu

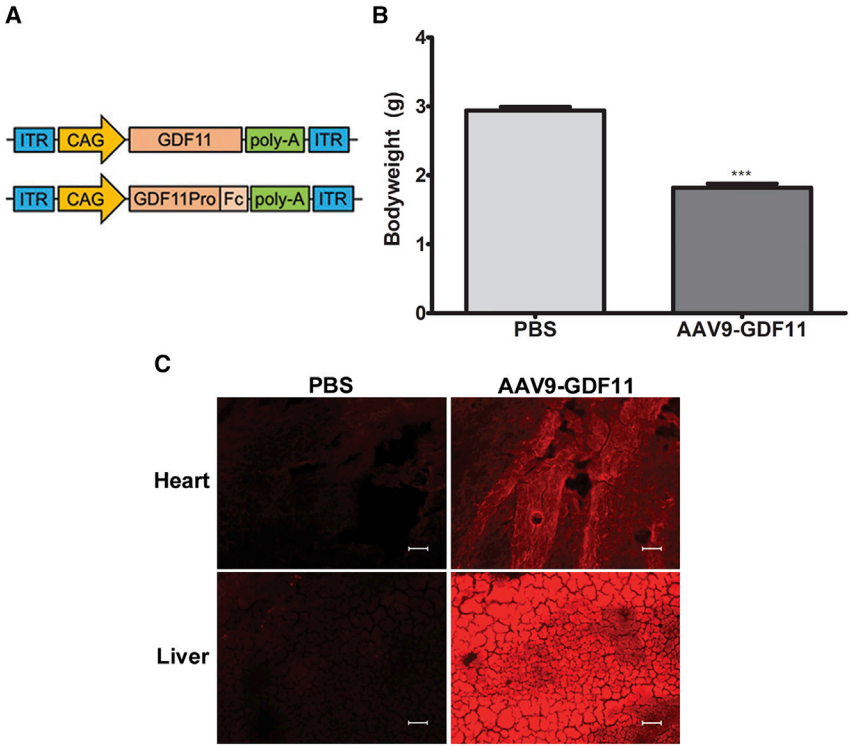

Figure 1. Reduced Body Mass in Neonatal Mice Induced by GDF11 Overexpression

(A) AAV9-GDF11 and AAV9-GDF11-Pro-Fc-1 vector design. The DNA gene sequence encoding for human GDF11 or human Fc-conjugated GDF11 propeptide wAS cloned into an AAV expression vector after a cytomegalovirus early enhancer/chicken β-actin (CAG) promoter with a polyadenylation signal. The entire sequence is flanked by two AAV inverted terminal repeats (ITRs). (B) Body weight of pups 10 days after treatment with 5×10^{11} vg AAV9-GDF11 or PBS control (n = 5). (C) Representative immunofluorescence sections from 14-day-old neonatal heart and liver sections stained for GDF11 (red). Scale bars, 50 μm. All error bars represent mean ± SEM. ***$p < 0.001$.

antigenicity, which may potentially contribute to unreliable observations.[24] For the present study, we chose to use gene delivery via adeno-associated virus (AAV) vectors to achieve systemic GDF11 overexpression. AAV-mediated gene delivery has been consistently shown to produce widespread and long-term gene expression in tissues such as liver, skeletal muscle, and heart. Proteins produced and secreted from host cells are expected to undergo a more natural maturation with proper protein folding and are, therefore, likely to exhibit higher activity and less immunogenicity. Furthermore, the AAV vector itself is non-pathogenic and does not provoke any measurable immune response.[25] To study the impact of GDF11 overexpression or blockade on skeletal muscle, we packaged the codon-optimized DNA sequence for human GDF11 or human Fc-conjugated GDF11 propeptide into AAV serotype 9 (AAV9) and assessed the effects in mouse skeletal muscle after neonatal intravenous administration. Here, we demonstrate that AAV9-mediated GDF11 overexpression inhibits skeletal muscle growth and causes corresponding reductions in muscle strength and endurance. Additionally, we show that GDF11 propeptide overexpression results in skeletal muscle hypertrophy and increased muscle strength without producing cardiac hypertrophy.

RESULTS

Excessive GDF11 Expression Causes Lethality

To study the impact of GDF11 overexpression, the codon-optimized DNA sequence encoding the full-length human GDF11 transgene was packaged into an AAV9 vector (AAV9-GDF11; Figure 1A; Figures S1 and S2A). To confirm proper transgene expression by the AAV9-GDF11 vector *in vitro*, HEK293 cells were infected with viral vectors, and the target protein was detected in whole cells by immunofluorescence and cell lysates by western blot (Figures S2B and S2C). For *in vivo* experiments, 3-day-old neonatal mice on a C57BL/6J background were intravenously administered 5×10^{11} vector genomes (vg) per mouse AAV9-GDF11 or PBS vehicle. Mice were followed closely after vector administration to assess treatment effect and identify signs of toxicity. Approximately 10 days after vector administration, mice treated with AAV9-GDF11 had an average body weight 38.1% lower than PBS-treated control mice (Figure 1B). By 14 days after injection, all mice treated with AAV9-GDF11 had either died or required euthanasia. Immunofluorescence analysis using a validated anti-human GDF11 antibody (R&D Systems, MAB19581, Minneapolis, MN, USA) revealed GDF11 expression in the neonatal liver and heart of mice treated with AAV9-GDF11 but not in PBS-treated control mice (Figure 1C).

GDF11 Overexpression Inhibits Skeletal Muscle Growth

Because AAV9-GDF11 was lethal at the initial treatment dose used, we titrated the AAV9-GDF11 treatment dose to determine a survivable dose. It was found that a 10-fold dose reduction from the initial dose of 5×10^{11} vg AAV9-GDF11 per mouse to 5×10^{10} vg AAV9-GDF11 per mouse was non-lethal. All mice that were administered this reduced dose of GDF11 survived to adulthood without any signs of overt toxicity, with the exception of reduced body mass. Mice treated with AAV9-GDF11 consistently weighed less than control mice at every time point tested, and at 16 weeks post-treatment, AAV9-GDF11-treated mice had an average total body weight 26.0% lower than PBS-treated controls (Figure 2A). Additionally, mice treated with AAV9-GDF11 demonstrated reduced forelimb strength and running endurance compared to PBS-treated controls, with a 43.4% and 25.3% decrease in grip strength and total distance traveled, respectively (Figures 2D and 2E). Differences in forelimb grip strength persisted even after normalizing force pulled to body weight (−34.6%; Figure 2F).

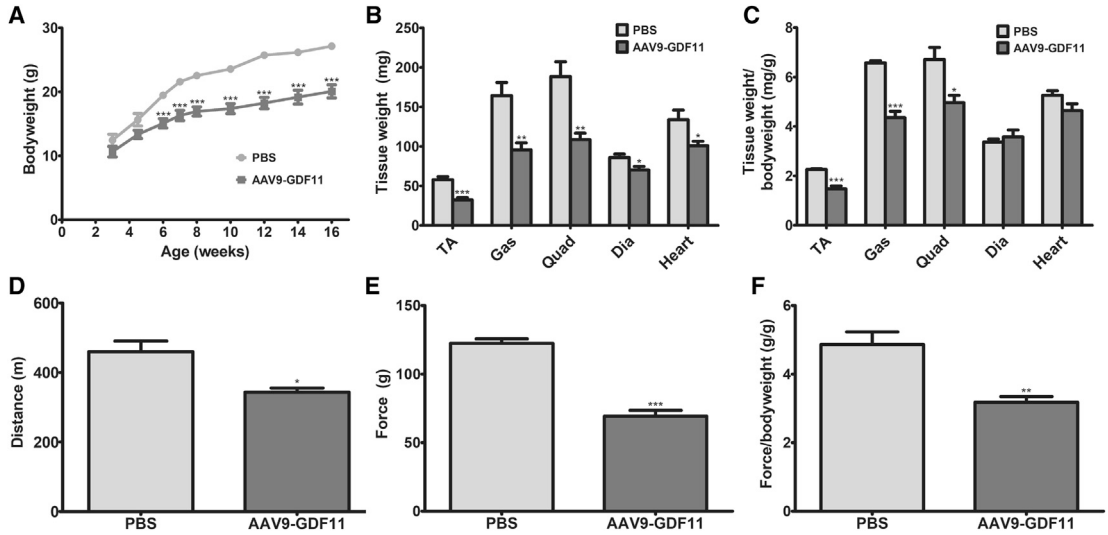

Figure 2. Effects of Neonatal GDF11 Administration on Muscle Mass and Function

3-day-old C57BL/6J pups were treated with 5×10^{10} vg AAV9-GDF11 or PBS control and followed for 16 weeks. (A) Body weight (n = 5). (B) Weight of whole limb muscles, diaphragm, and heart and (C) weight normalized to body weight (n = 5). (D) Total distance traveled on the treadmill running test (n = 5). Depicted data represent total distance traveled at 14 weeks post-treatment. (E) Peak force produced on the forelimb grip strength test and (F) peak force normalized to body weight (n = 5). Depicted data represent peak force reading at 16 weeks post-treatment. All error bars represent mean ± SEM. *p < 0.05; **p < 0.01; ***p < 0.001.

16 weeks after treatment, the whole tibialis anterior (TA), gastrocnemius, quadriceps, diaphragm, and heart were extracted for analysis. In AAV9-GDF11-treated mice, limb muscles weighed significantly less compared to those of control mice, with an observed −43.9%, −42.6% and −35.1% difference in TA mass, gastrocnemius mass, and quadriceps mass, respectively. A difference of −16.5% and −24.7% in diaphragm mass and heart mass, respectively, was also observed with AAV9-GDF11 treatment (Figure 2B). The difference in diaphragm mass paralleled a decreased diaphragm myofiber diameter in mice treated with AAV9-GDF11 (Figure S3). However, when tissue weight was normalized to body weight, there was no statistically significant difference seen in diaphragm or heart (−11.8%; p = 0.0984 for normalized heart mass), although normalized limb muscle mass remained significantly different (−34.8%, −33.8%, and −26.1% difference in normalized TA mass, normalized gastrocnemius mass, and normalized quadriceps mass, respectively; Figure 2C). Additionally, no difference was observed in abdominal fat pad mass (348.7 mg ± 62.3 mg and 357.5 mg ± 107.5 mg in mice treated with PBS or AAV9-GDF11, respectively) or in supraclavicular brown fat mass between the experimental groups (122.2 mg ± 9.6 mg and 130.6 mg ± 18.5 mg in mice treated with PBS or AAV9-GDF11, respectively; Figures S4A and S4B).

H&E staining and immunofluorescence analysis of the quadriceps muscles using an anti-laminin α2 primary antibody to stain individual muscle fibers showed a significantly left-shifted minimum Feret diameter (MFD) distribution in samples from mice treated with AAV9-GDF11 (Figures 3A–3C). The median MFDs in quadriceps myofibers were 57.35 μm (interquartile range [IQR], 46.47 μm to 68.27 μm) and 38.73 μm (IQR, 30.02 μm to 49.72 μm) for PBS-treated and AAV9-GDF11-treated mice, respectively (Figure 3D). Western blot analysis of heart, liver, and quadriceps homogenates revealed a band corresponding to full-length GDF11 (~45 kDa), whereas no band was observed in corresponding samples from PBS-treated control mice (Figure 3E).[26,27]

We next sought to determine whether GDF11 overexpression led to upregulation of TGF-β-SMAD2/3 signaling in skeletal muscle. The bands for phosphorylated SMAD3 (pSMAD3) (~48 kDa) and SMAD3 (~48 kDa) were detected at the expected size. Western blot analysis showed a 2.2-fold increase in pSMAD3 protein in gastrocnemius samples from mice treated with AAV9-GDF11, while protein levels of total SMAD3 were not significantly different between AAV9-GDF11-treated mice and PBS-treated mice (Figure 4B). Additionally, immunofluorescence analysis in gastrocnemius muscle sections revealed an increase of 41.8% in the proportion of pSMAD2/3$^+$ nuclei to total nuclei in mice treated with AAV9-GDF11 compared to PBS-treated mice (Figures 4C and 4D).

Fc-Conjugated GDF11 Propeptide Overexpression Enhances Skeletal Muscle Growth without Affecting Heart Mass

Given the hindering effects of GDF11 on muscle growth and function, we next aimed to determine whether GDF11 blockade by GDF11 propeptide could enhance muscle growth. The effector protein GDF11 propeptide was fused to human immunoglobulin (Ig)G1 Fc (GDF11Pro-Fc-1) to prolong factor half-life in circulation and also to facilitate identification by an anti-human Fc antibody. The DNA sequence encoding the GDF11Pro-Fc-1 gene was then packaged into AAV9 vector (AAV9-GDF11Pro-Fc-1; Figure 1A; Figures S1 and S2A). For *in vivo* experiments, 3-day-old neonatal mice were

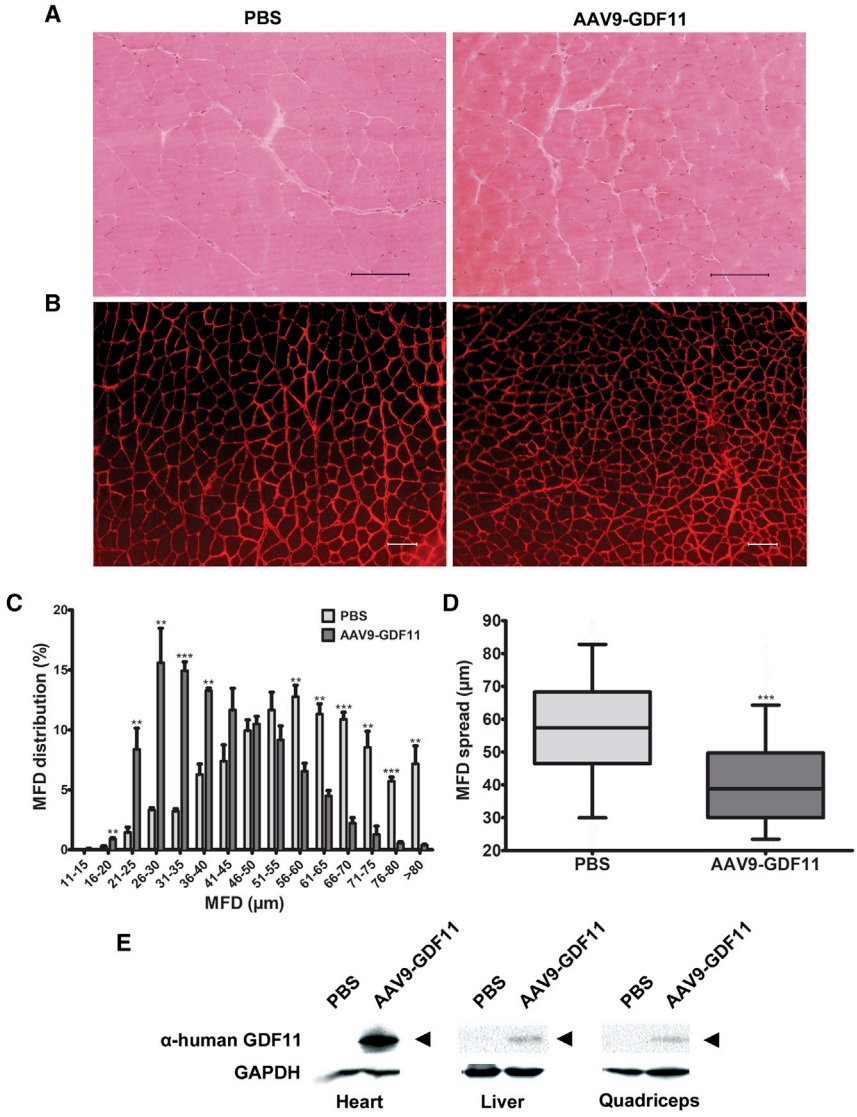

Figure 3. GDF11 Overexpression Inhibits Skeletal Muscle Growth

(A) Representative H&E sections and (B) immunofluorescence sections from quadriceps sections. Laminin-α2 staining was used to visualize individual myofibers. Scale bars, 100 μm. (C) Mean distribution of myofiber MFD in quadriceps muscle. 600 myofibers were measured per mouse (n = 3). Error bars represent mean ± SEM. $^{**}p < 0.01$; $^{***}p < 0.001$. (D) Box-and-whiskers plot of myofiber MFD spread in quadriceps (n = 3). Box represents the interquartile range (IQR), with the middle line representing the 50th percentile. The lower and upper whisker boundaries represent the 5th and 95th percentiles, respectively. $^{***}p < 0.001$. (E) Western blot analysis revealed the expected band corresponding to full-length GDF11 (~45 kDa; black arrows) in tissue homogenates in the AAV9-GDF11 group. GAPDH was used as a loading control.

intravenously administered the AAV9-GDF11Pro-Fc-1 vector at a dose of 5×10^{11} vg per mouse or PBS vehicle. Both treated and control mice survived to adulthood and showed no signs of toxicity. The AAV9-GDF11Pro-Fc-1 group exhibited significantly increased body mass compared to the PBS-treated control group (+24.2%; Figure 5A). Mice treated with AAV9-GDF11Pro-Fc-1 demonstrated a 34.9% increase in force pulled on a forelimb grip strength test compared to control mice, which changed to a 7.7% increase when force pulled was normalized to body weight (p = 0.0344; Figures 5E and 5F). However, a significant difference was not observed on running endurance by the treadmill running test (Figure 5D).

At 28 weeks of age, whole TA, gastrocnemius, quadriceps, diaphragm, and heart samples were collected. Limb muscle mass and diaphragm mass in the AAV9-GDF11Pro-Fc-1 group were higher than those of corresponding PBS-treated control mice (+30.6%, +17.8%, +20.2% and +21.1% difference in TA mass, gastrocnemius mass, quadriceps mass, and diaphragm mass, respectively; Figure 5B). However, there was no difference observed in the ratio of tissue weight to body weight (Figure 5C). Also, no difference was observed in abdominal adipose tissue mass (397.7 mg ± 98.7 mg and 544.5 mg ± 115.0 mg in mice treated with PBS or AAV9-GDF11Pro-Fc-1, respectively) or in supraclavicular brown fat mass between the groups (122.2 mg ± 17.9 mg and 148.4 mg ± 22.0 mg in mice treated with PBS or AAV9-GDF11Pro-Fc-1, respectively; Figures S4C and S4D).

H&E analysis and muscle fiber staining using an anti-laminin α2 antibody showed significant muscle hypertrophy in mice treated with AAV9-GDF11Pro-Fc-1, as evidenced by a right-shifted MFD distribution in comparison to PBS-treated control mice (Figures 6A–6C). The median MFD in the PBS-treated group was 51.39 μm (IQR, 39.41 μm to 64.29 μm), while the median MFD in the GDF11 propeptide-Fc-treated group was 62.19 μm (IQR, 48.45 μm to 73.51 μm; Figure 6D). Western blot analysis of heart, liver, and quadriceps detected a band corresponding to full-length GDF11Pro-Fc-1 (~57 kDa) protein only in the heart and liver of mice treated with AAV9-GDF11Pro-Fc-1. Additionally, a major degradation product containing the human Fc was observed in heart, liver, and quadriceps samples (~32 kDa), while no equivalent bands were observed in the heart, liver, or quadriceps samples from the PBS-treated group (Figure 6E).

DISCUSSION

In the present study, we show that GDF11 overexpression via AAV9-mediated gene delivery in neonatal mice inhibits skeletal muscle growth and causes reductions in forelimb grip strength and running endurance. Additionally, we report decreased heart mass with

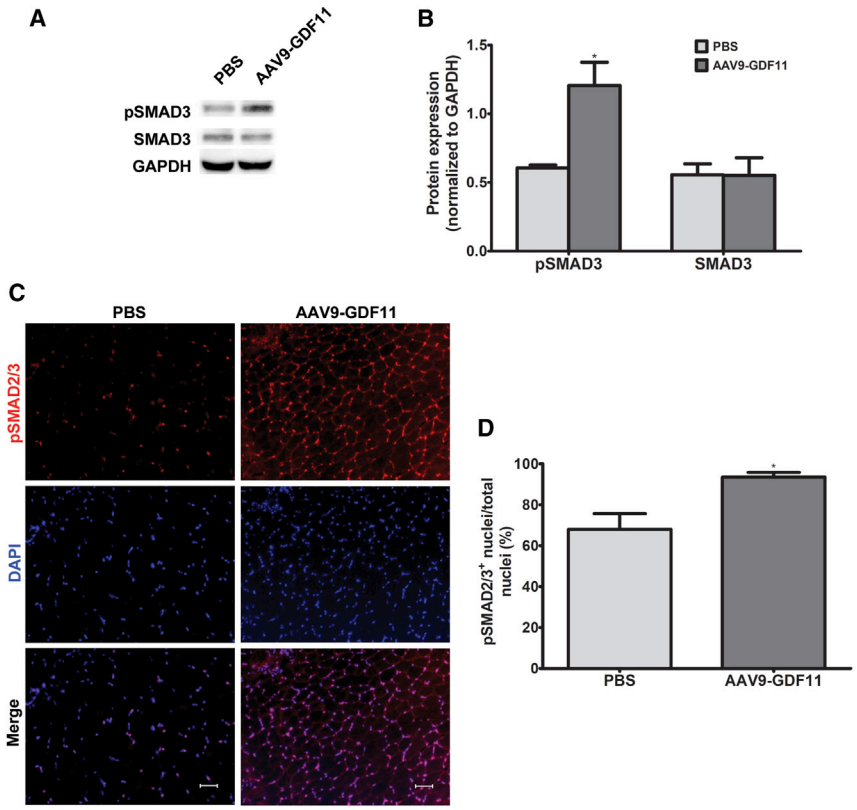

Figure 4. GDF11 Activates the TGF-β-SMAD2/3 Pathway

(A) Representative western blot analysis of SMAD3 signaling. (B) Semiquantitative analysis of relative pSMAD3 and SMAD3 protein levels normalized to GAPDH (n = 2–3). (C) Representative immunofluorescence sections from gastrocnemius stained for pSMAD2/3 (red). Nuclei were stained with DAPI (blue). Scale bars, 50 μm. (D) Percentage of SMAD2/3$^+$ nuclei in relation to total nuclei (n = 3). All error bars represent mean ± SEM. *p < 0.05.

GDF11 overexpression. On the contrary, GDF11 propeptide induces a modest increase in skeletal muscle growth and forelimb grip strength. Earlier reports identified GDF11 as a factor capable of increasing strength and reversing functional impairment in aged skeletal muscle.[12] From a mechanistic standpoint, GDF11, similarly to myostatin, would be expected to negatively regulate skeletal muscle growth *in vivo* by signaling through the canonical TGF-β-SMAD2/3 pathway. Overall, our findings agree with the view that activation of the TGF-β-SMAD2/3 pathway by GDF11 has inhibitory effects on skeletal muscle growth.[17]

Several *in vitro* and *in vivo* studies suggest ActRII-mediated activation of the TGF-β-SMAD2/3 pathway inhibits myogenesis and inhibition of ActRII induces skeletal muscle hypertrophy.[28–32] It is, therefore, reasonable to predict that blockade of ActRII-binding ligands such as GDF11 would lead to reduced inhibition of skeletal muscle growth, and our results with AAV9-GDF11Pro-Fc-1 confirm that hypothesis. Similar results in skeletal muscle have also been observed with myostatin inhibitors such as myostatin propeptide and follistatin.[16,32–35] Our data show that treatment with GDF11 propeptide may augment skeletal muscle growth and forelimb grip strength, albeit not substantially in our trial, as the observed difference in muscle mass disappears when muscle mass is normalized to body mass. Furthermore, there is only a small difference in forelimb grip strength between treatment and control when grip force is normalized to body mass. Even so, the increase in muscle mass is at least proportional to the increase in body mass, which suggests that muscle growth is a major contributor to the change in body mass. To explain these results, it is possible that the dose of AAV9-GDF11Pro-Fc-1 vector used in this study is insufficient to cause a hypertrophic effect large enough to be measurable in the muscle mass/body mass ratio, as western blot analysis reveals considerable degradation of the GDF11 propeptide *in vivo*. If desired, we predict that enhanced skeletal muscle growth may be achieved by the addition of a mutation (D120A) into the GDF11 propeptide gene to impart resistance to *in vivo* protease degradation of the active protein in order to extend its half life.[5] Additionally, due to the close similarities between GDF11 and myostatin, it is likely that GDF11 propeptide exerts its hypertrophic effects in muscle via both GDF11 and myostatin inhibition, as GDF11 propeptide has shown inhibitory effects on myostatin *in vitro*.[5] Lastly, despite increases in skeletal muscle mass and forelimb grip strength, we do not see any signs of cardiac hypertrophy in mice treated with GDF11 propeptide. A similar observation was reported in a previous study examining the effects of myostatin propeptide on skeletal muscle and heart.[32] This may be explained by differences in signal transduction and, possibly, negative-feedback regulation between skeletal and cardiac muscle, and these tissue-specific distinctions should be more closely examined.

GDF11 has previously been reported to improve skeletal muscle mass and strength in aged mice.[12] In order to evaluate the true effects of GDF11 in the context of aging, it is important to take into consideration potential age-specific differences that may influence effects of GDF11. The present study only examined GDF11 overexpression and blockade in young mice, and that is a major limitation of this dataset. Levels of endogenous circulating GDF11 are suggested to change with increasing age, and the value of restoring GDF11 levels in old age is not clear.[17,36] Future studies should examine the effect of GDF11 overexpression or blockade in aging models to identify age-specific differences. Decreased skeletal muscle mass and strength are among the characteristics observed in old mice, and it will be interesting to see what effect GDF11 or GDF11 propeptide overexpression would have on those features.[37–39]

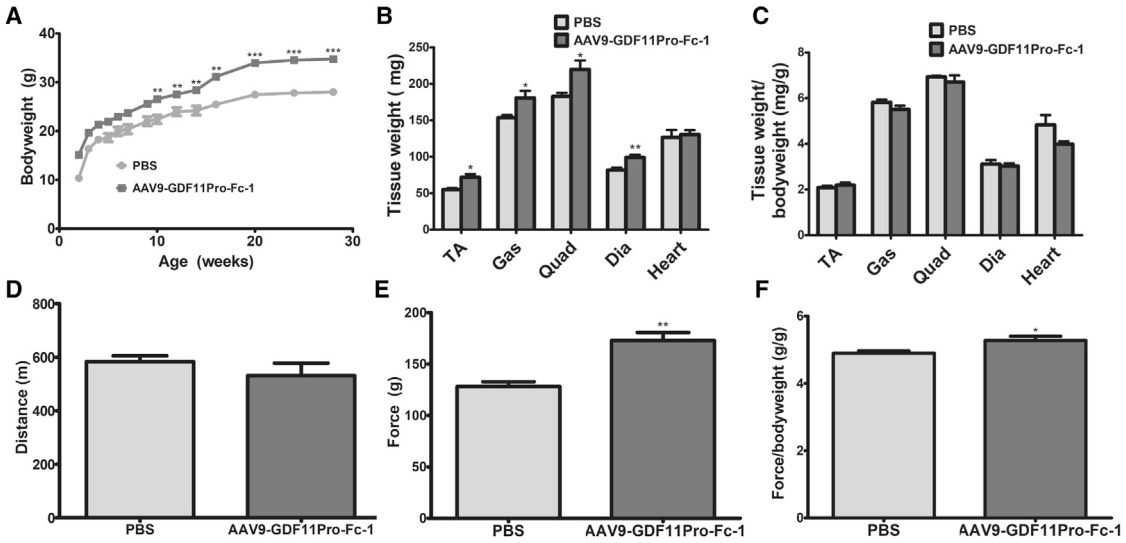

Figure 5. Effects of Neonatal GDF11 Propeptide Administration on Muscle Mass and Function

3-day-old C57BL/6J pups were treated with 5×10^{11} vg AAV9-GDF11Pro-Fc-1 or PBS control and followed for 28 weeks. (A) Body weight (n = 5). (B) Weight of whole limb muscles, diaphragm, and heart and (C) weight normalized to body weight (n = 5). (D) Total distance traveled on the treadmill running test (n = 5). Depicted data represent total distance traveled at 26 weeks post-treatment. (E) Peak force produced on the forelimb grip strength test and (F) peak force normalized to body weight (n = 5). Depicted data represent peak force reading at 28 weeks post-treatment. All error bars represent mean ± SEM. *p < 0.05; **p < 0.01; ***p < 0.001.

Another point to consider is that GDF11 may exhibit unique effects via alternative pathways such as Ras/ERK, PI3K/Akt/FOXO, and p38 MAPK.[21,40] However, the significance and consequence of these alternative pathways remains to be elucidated. These potentially unique mechanisms of GDF11 need to be further explored, specifically factors that differentiate GDF11 from other TGF-β ligands, such as myostatin.

There are several limitations to this study that leave unanswered questions. First, AAV9 achieves widespread transgene expression in the liver, lungs, heart, skeletal muscle, and CNS after systemic administration. Therefore, we cannot yet conclude whether the observed effects in muscle are primarily due to local effect in the muscle tissue or a by-product of a systemic response to GDF11 overexpression. TGF-β signaling has roles across multiple organs in the body, and it is understood that GDF11 overexpression or blockade mediates potentially variable effects across different organs such as the brain, heart, and endothelial tissue.[41] Additionally, we cannot exclude the possibility that GDF11-induced anorexia may have contributed to inhibited muscle growth in AAV9-GDF11-treated mice because food intake was not measured in this study. Given that fat mass does not change significantly with GDF11 treatment, we do not predict that anorexia is a major contributor to the observed phenotype. Finally, the systemic targeting by AAV9 may influence expression of other circulating factors with undetermined effects.

Here, we present a method of studying GDF11 *in vivo* using an AAV vector to achieve long-term factor expression after only a single dose. This gene delivery strategy circumvents the need for daily injections of expensive rGDF11 protein used in previous studies.[12,42] In summation, the results of this study and several other recent reports indicate that GDF11 has a detrimental effect on skeletal muscle growth and function.[19,20] Conversely, treatment with the GDF11 propeptide appears to augment skeletal muscle growth and increase strength without causing undesirable cardiac hypertrophy.

MATERIALS AND METHODS

Plasmid Construction and AAV Vector Production

The sequence for human IgG1-Fc was inserted at the C terminus of the human GDF11 propeptide sequence to form the GDF11Pro-Fc-1 fusion protein sequence. Sequences encoding codon-optimized GDF11 and GDF11Pro-Fc-1 were synthesized (GenScript, Piscataway, NJ, USA) and cloned into the AAV backbone under the transcriptional control of the ubiquitous CAG promoter (consisting of the cytomegalovirus [CMV] enhancer, chicken β-actin promoter, and a globin intron).[43] AAV9 vectors were generated by the triple plasmid transfection method in HEK293 cells.[44] Vectors were purified from cell lysate and medium by polyethylene glycol (PEG) precipitation followed by two rounds of CsCl density ultracentrifugation. Titers of purified viral stock determined by DNA dot blot were in the range of 5×10^{12} to 1×10^{13} vg/mL. Vector infectivity and proper transgene expression of purified vectors were confirmed by *in vitro* reinfection in HEK293 cells at an MOI of 10,000 vg per cell. 5 to 10 μM Hoechst 33342 was co-administered into HEK293 cells to facilitate transgene expression.[45] Proper transgene expression was verified by immunofluorescence and western blot in transiently transfected HEK293 cells, using a monoclonal mouse anti-human GDF11 antibody (R&D Systems, MAB19581, Minneapolis, MN, USA) and a polyclonal goat anti-human IgG Fc-specific (Sigma-Aldrich, I2136) antibody for GDF11 and GDF11Pro-Fc-1, respectively.

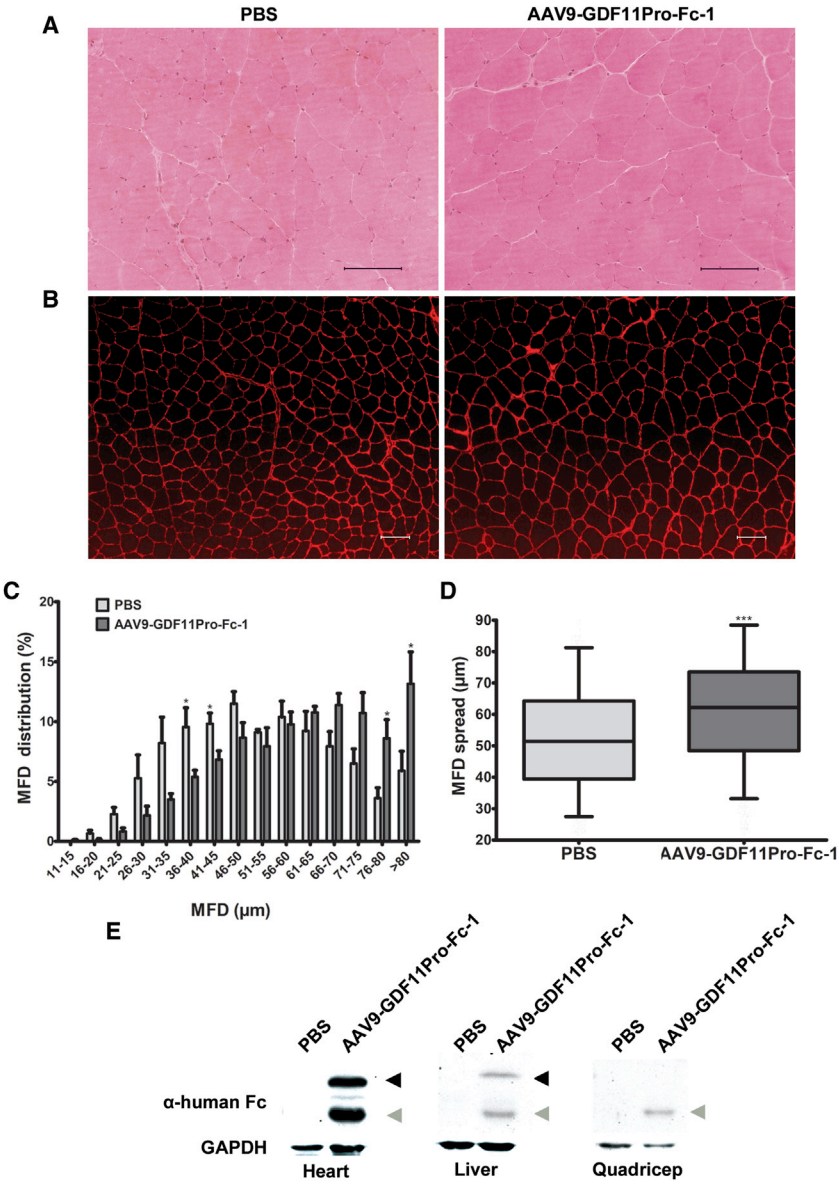

Figure 6. GDF11 Propeptide-Fc Enhances Skeletal Muscle Growth

(A) Representative H&E sections and (B) immunofluorescence sections from quadriceps sections. Laminin-α2 staining was used to visualize individual myofibers. Scale bars, 100 μm. (C) Mean distribution of myofiber MFD in quadriceps muscle. 600 myofibers were measured per mouse (n = 5). Error bars represent mean ± SEM. *$p < 0.05$. (D) Box-and-whiskers plot of myofiber MFD spread in quadriceps (n = 5). Box represents the interquartile range (IQR), with the middle line representing the 50th percentile. The lower and upper whisker boundaries represent the 5th and 95th percentiles, respectively. ***$p < 0.001$. (E) Western blot analysis revealed the expected band corresponding to full-length GDF11Pro-Fc-1 (~57 kDa; black arrows) in tissue homogenates from heart and liver in the AAV9-GDF11Pro-Fc-1 group. The corresponding band could not be detected in GDF11 propeptide-Fc-treated quadriceps samples. An additional band was recognized at ~32 kDa (gray arrows) in GDF11 propeptide-Fc-treated heart, liver, and quadriceps that was not present in PBS-treated samples. GAPDH was used as loading control.

Mice and AAV Vector Administration

Mice were maintained in a 12-hr:12-hr light:dark artificial light cycle (0700–1900 hr) at a temperature of 20°C and a humidity of 55 ± 5%. All animal protocols were approved by the University of North Carolina Animal Care and Use Committee. Sample size determination was based on power analyses from previous studies and literature review. Neonatal mice (3 days of age) on a C57BL6J background were randomly allocated into experimental groups and treated by temporal vein injection, with doses ranging from 5×10^{10} to 5×10^{11} vg per mouse of AAV9-GDF11, AAV9-GDF11Pro-Fc-1, or PBS in a 50-μL volume. Treated mice were weaned at 3 weeks of age. Mice had *ad libitum* access to food and water. Body weight was assessed at weaning and every week initially. As weight gain became more gradual, body weight measurements were taken bimonthly to monthly. AAV9-GDF11- and AAV9-GDF11Pro-Fc-1-treated mice were sacrificed at 16 weeks and 28 weeks, respectively. For non-survival surgery, mice were anesthesized with 2.5% 2,2,2-tribromoethanol (Avertin) at a dose of 350 mg/kg. The entire heart, diaphragm, gastrocnemius, TA, hamstring, and quadriceps muscles were surgically removed, snap frozen in 2-methylbutane, and stored at −80°C.

Muscle Functional Testing

Mice were trained and acclimated to grip strength and treadmill apparatuses prior to data collection. Before testing, experimental groups were anonymized. The grip strength device (Columbus Instruments, Columbus, OH, USA) measured tension peak force. The mouse was allowed to rest its front forepaws on the bar until the bar was evenly grasped with both forepaws. Then the mouse tail was pulled back slowly until the mouse released its grip on the bar. The maximal force pulled by the mouse in grams was recorded. A minimum of 5 measurements at 1-min intervals were obtained at testing for each mouse, and the highest value obtained was used for statistical analysis. The treadmill apparatus (Harvard Apparatus, Holliston, MA, USA) was placed on a 15° incline, with the shock pad set to 1 mA. Starting speed was set at 5 m/min for 1 min. The speed was then gradually increased to 10 m/min for 5 min and continually increased in 5-m/min increments every 5 min. A mouse was removed when it failed to re-enter the treadmill after 7 s. Total distance traveled was used for statistical analysis. Grip strength and treadmill tests were conducted by a single experimenter blinded to the experimental groups.

H&E Staining

10-μm transverse cryosections were prepared from snap-frozen quadriceps samples. Sections were fixed with 3% acetic acid in 95% ethanol and washed in tap water. Sections were subsequently stained with Gill's hematoxylin #3 for 20 min and washed with tap water to blue. Sections were differentiated in 1% acid alcohol for 10 s and washed with tap water. Sections were blued in 0.2% ammonia water for 30 s and washed with tap water. Eosin counterstain was applied for 5 s, and excess eosin was washed off with tap water. Slides were dehydrated for 2 min each in 70%, 85%, 95%, and 100% ethanol and dried. Sections were immersed in xylene for at least 5 min, and slides were mounted with Permount (Thermo-Fisher, SP 15-100). A Nikon Eclipse TE300 microscope (Nikon USA, Melville, NY, USA) was used to visualize sections, and images were captured with a SPOT RT Slider camera (Diagnostic Instruments, Sterling Heights, MI, USA).

Immunofluorescence Analysis

10-μm transverse cryosections were prepared from snap-frozen quadriceps samples. Sections were blocked with 10% horse serum in PBS and stained with rat monoclonal anti-laminin α2 antibody (1:500; Sigma-Aldrich, L0663) for 1 hr. Sections were washed three times with PBS and Cy3-conjugated anti-rat IgG (1:5,000) was added for 1 hour. Slides were washed again with PBS, and coverslips were affixed with Gel-Mount aqueous mounting media (Biomeda, Foster City, CA, USA). A Nikon Eclipse TE300 microscope (Nikon USA, Melville, NY, USA) was used to visualize individual muscle fibers. Images were captured at 10× magnification with a SPOT RT Slider camera (Diagnostic Instruments, Sterling Heights, MI, USA) for fiber diameter analysis. ImageJ software was used to outline individual myofibers and determine MFD in 600 myofibers per mouse. For pSMAD2/3 staining, all steps were as described, with the exception of an additional permeabilization step prior to blocking with 0.2% Triton X-100 for 30 min. Sections for pSMAD2/3 staining were incubated with rabbit anti-pSMAD2/3 antibody (1:500; Santa Cruz Biotechnology, sc-117691) overnight, washed three times with PBS, and incubated with Cy3-conjugated anti-rabbit IgG (1:1,000) for 1 hr. Percentage of $pSMAD2/3^{+}$ nuclei was calculated from at least 1,000 nuclei per mouse. Image captures were anonymized, and the investigator conducting immunofluorescence analysis was blinded to the experimental group.

Western Blot

Snap-frozen samples from heart, quadriceps, and liver were finely homogenized in RIPA buffer (150 mM NaCl, 1% Triton X-100, 0.5% sodium deoxycholate, 0.1% SDS, 50 mM Tris [pH 7.5], 1 mM PMSF) with protease inhibitor cocktail (Sigma-Aldrich, St. Louis, MO, USA) and briefly sonicated to shear genomic DNA. Samples were centrifuged at 13,000 rpm for 15 min to pellet unsolubilized DNA, and the concentration of the supernatant was determined by bicinchoninic acid assay (BCA). Protein samples were diluted to the same concentration and reduced in SDS-PAGE loading buffer (62.5 mM Tris-HCl [pH 6.8], 1.5% SDS, 8.3% glycerol, 1.5% β-mercaptoethanol, 0.005% bromophenol blue). Approximately 40 μg protein was loaded per lane. Samples were separated at 80–120 V on a 12% SDS-PAGE gel and transferred to a 0.2-μm polyvinylidene fluoride (PVDF) membrane. 5% non-fat dry milk in TBS-T (10 mmol/L Tris-HCl [pH 7.5], 100 mmol/L NaCl, and 0.1% Tween 20) was used to block the membrane. Primary antibodies were incubated with the membrane overnight. The membrane was washed in TBS-T three times, and appropriate horseradish peroxidase (HRP)-conjugated antibodies were incubated for 1 hr. The membrane was washed in TBS-T five times and developed with Western Lightning ECL Pro (PerkinElmer, Waltham, MA, USA). Primary antibodies used were anti-human GDF11 (1:5,000; R&D Systems, MAB19581, Minneapolis, MN, USA), anti-human IgG Fc specific (1:5,000; Sigma-Aldrich, I2136), anti-pSmad3 (S423/425; 1:1,000; Abcam, ab52903), anti-Smad3 (1:1,000; Abcam, ab28379), and anti-mouse GAPDH (1:10,000; Sigma-Aldrich, G9545).

Statistical Analysis

Statistical values are given as mean ± SEM, except where indicated. Student's t test was used to compare two groups. One-way ANOVA was used to compare three or more groups. Mann-Whitney U test was used specifically to compare overall myofiber MFD distribution between two groups. Graphs and statistical analysis were produced using GraphPad Prism 5.0 (GraphPad Software, La Jolla, CA, USA). $p < 0.05$ was considered statistically significant.

SUPPLEMENTAL INFORMATION

Supplemental Information includes four figures and can be found with this article online at https://doi.org/10.1016/j.ymthe.2018.01.016.

AUTHOR CONTRIBUTIONS

Conceptualization, Q.J. and X.X.; Methodology, Q.J., C.Q., and X.X.; Investigation, Q.J., C.Q., and Jianbin Li; Writing – Original Draft, Q.J. and X.X.; Writing – Reviewing & Editing, Q.J., C.Q., and X.X.; Resources, Juan Li and X.X.; Supervision, Juan Li and X.X.; Funding Acquisition, X.X.

CONFLICTS OF INTEREST

The authors declare no conflict of interest.

ACKNOWLEDGMENTS

This work was supported by NIH grants R01NS079568 and R01NS082536 to X.X. and an Eshelman Institute of Innovation award to X.X. We thank Dr. Karen Bulaklak for critical reading of the manuscript.

REFERENCES

1. Wu, M.Y., and Hill, C.S. (2009). TGF-β superfamily signaling in embryonic development and homeostasis. Dev. Cell *16*, 329–343.

2. Burks, T.N., and Cohn, R.D. (2011). Role of TGF-β signaling in inherited and acquired myopathies. Skelet. Muscle *1*, 19.

3. Accornero, F., Kanisicak, O., Tjondrokoesoemo, A., Attia, A.C., McNally, E.M., and Molkentin, J.D. (2014). Myofiber-specific inhibition of TGFβ signaling protects skeletal muscle from injury and dystrophic disease in mice. Hum. Mol. Genet. *23*, 6903–6915.

4. Li, Z., Kawasumi, M., Zhao, B., Moisyadi, S., and Yang, J. (2010). Transgenic over-expression of growth differentiation factor 11 propeptide in skeleton results

in transformation of the seventh cervical vertebra into a thoracic vertebra. Mol. Reprod. Dev. *77*, 990–997.

5. Ge, G., Hopkins, D.R., Ho, W.-B., and Greenspan, D.S. (2005). GDF11 forms a bone morphogenetic protein 1-activated latent complex that can modulate nerve growth factor-induced differentiation of PC12 cells. Mol. Cell. Biol. *25*, 5846–5858.

6. McPherron, A.C., Lawler, A.M., and Lee, S.J. (1999). Regulation of anterior/posterior patterning of the axial skeleton by growth/differentiation factor 11. Nat. Genet. *22*, 260–264.

7. Esquela, A.F., and Lee, S.J. (2003). Regulation of metanephric kidney development by growth/differentiation factor 11. Dev. Biol. *257*, 356–370.

8. Kim, J., Wu, H.H., Lander, A.D., Lyons, K.M., Matzuk, M.M., and Calof, A.L. (2005). GDF11 controls the timing of progenitor cell competence in developing retina. Science *308*, 1927–1930.

9. Harmon, E.B., Apelqvist, A.A., Smart, N.G., Gu, X., Osborne, D.H., and Kim, S.K. (2004). GDF11 modulates NGN3+ islet progenitor cell number and promotes beta-cell differentiation in pancreas development. Development *131*, 6163–6174.

10. Wu, H.-H., Ivkovic, S., Murray, R.C., Jaramillo, S., Lyons, K.M., Johnson, J.E., and Calof, A.L. (2003). Autoregulation of neurogenesis by GDF11. Neuron *37*, 197–207.

11. Loffredo, F.S., Steinhauser, M.L., Jay, S.M., Gannon, J., Pancoast, J.R., Yalamanchi, P., Sinha, M., Dall'Osso, C., Khong, D., Shadrach, J.L., et al. (2013). Growth differentiation factor 11 is a circulating factor that reverses age-related cardiac hypertrophy. Cell *153*, 828–839.

12. Sinha, M., Jang, Y.C., Oh, J., Khong, D., Wu, E.Y., Manohar, R., Miller, C., Regalado, S.G., Loffredo, F.S., Pancoast, J.R., et al. (2014). Restoring systemic GDF11 levels reverses age-related dysfunction in mouse skeletal muscle. Science *344*, 649–652.

13. Katsimpardi, L., Litterman, N.K., Schein, P.A., Miller, C.M., Loffredo, F.S., Wojtkiewicz, G.R., Chen, J.W., Lee, R.T., Wagers, A.J., and Rubin, L.L. (2014). Vascular and neurogenic rejuvenation of the aging mouse brain by young systemic factors. Science *344*, 630–634.

14. Nakashima, M., Toyono, T., Akamine, A., and Joyner, A. (1999). Expression of growth/differentiation factor 11, a new member of the BMP/TGFbeta superfamily during mouse embryogenesis. Mech. Dev. *80*, 185–189.

15. Oh, S.P., Yeo, C.Y., Lee, Y., Schrewe, H., Whitman, M., and Li, E. (2002). Activin type IIA and IIB receptors mediate Gdf11 signaling in axial vertebral patterning. Genes Dev. *16*, 2749–2754.

16. Lee, S.-J., and McPherron, A.C. (2001). Regulation of myostatin activity and muscle growth. Proc. Natl. Acad. Sci. USA *98*, 9306–9311.

17. Egerman, M.A., Cadena, S.M., Gilbert, J.A., Meyer, A., Nelson, H.N., Swalley, S.E., Mallozzi, C., Jacobi, C., Jennings, L.L., Clay, I., et al. (2015). GDF11 increases with age and inhibits skeletal muscle regeneration. Cell Metab. *22*, 164–174.

18. Smith, S.C., Zhang, X., Zhang, X., Gross, P., Starosta, T., Mohsin, S., Franti, M., Gupta, P., Hayes, D., Myzithras, M., et al. (2015). GDF11 does not rescue aging-related pathological hypertrophy. Circ. Res. *117*, 926–932.

19. Hammers, D.W., Merscham-Banda, M., Hsiao, J.Y., Engst, S., Hartman, J.J., and Sweeney, H.L. (2017). Supraphysiological levels of GDF11 induce striated muscle atrophy. EMBO Mol. Med. *9*, 531–544.

20. Zimmers, T.A., Jiang, Y., Wang, M., Liang, T.W., Rupert, J.E., Au, E.D., Marino, F.E., Couch, M.E., and Koniaris, L.G. (2017). Exogenous GDF11 induces cardiac and skeletal muscle dysfunction and wasting. Basic Res. Cardiol. *112*, 48.

21. Walker, R.G., Poggioli, T., Katsimpardi, L., Buchanan, S.M., Oh, J., Wattrus, S., Heidecker, B., Fong, Y.W., Rubin, L.L., Ganz, P., et al. (2016). Biochemistry and biology of GDF11 and myostatin: similarities, differences, and questions for future investigation. Circ. Res. *118*, 1125–1142.

22. Harper, S.C., Brack, A., MacDonnell, S., Franti, M., Olwin, B.B., Bailey, B.A., Rudnicki, M.A., and Houser, S.R. (2016). Is growth differentiation factor 11 a realistic therapeutic for aging-dependent muscle defects? Circ. Res. *118*, 1143–1150.

23. Hinken, A.C., Powers, J.M., Luo, G., Holt, J.A., Billin, A.N., and Russell, A.J. (2016). Lack of evidence for GDF11 as a rejuvenator of aged skeletal muscle satellite cells. Aging Cell *15*, 582–584.

24. Rosano, G.L., and Ceccarelli, E.A. (2014). Recombinant protein expression in *Escherichia coli*: advances and challenges. Front. Microbiol. *5*, 172.

25. Samulski, R.J., and Muzyczka, N. (2014). AAV-mediated gene therapy for research and therapeutic purposes. Annu. Rev. Virol. *1*, 427–451.

26. Pacak, C.A., Sakai, Y., Thattaliyath, B.D., Mah, C.S., and Byrne, B.J. (2008). Tissue specific promoters improve specificity of AAV9 mediated transgene expression following intra-vascular gene delivery in neonatal mice. Genet. Vaccines Ther. *6*, 13.

27. Pacak, C.A., Mah, C.S., Thattaliyath, B.D., Conlon, T.J., Lewis, M.A., Cloutier, D.E., Zolotukhin, I., Tarantal, A.F., and Byrne, B.J. (2006). Recombinant adeno-associated virus serotype 9 leads to preferential cardiac transduction in vivo. Circ. Res. *99*, e3–e9.

28. Lach-Trifilieff, E., Minetti, G.C., Sheppard, K., Ibebunjo, C., Feige, J.N., Hartmann, S., Brachat, S., Rivet, H., Koelbing, C., Morvan, F., et al. (2014). An antibody blocking activin type II receptors induces strong skeletal muscle hypertrophy and protects from atrophy. Mol. Cell. Biol. *34*, 606–618.

29. Hu, S., Chen, C., Sheng, J., Sun, Y., Cao, X., and Qiao, J. (2010). Enhanced muscle growth by plasmid-mediated delivery of myostatin propeptide. J. Biomed. Biotechnol. *2010*, Article ID 862591.

30. Zhu, J., Li, Y., Lu, A., Gharaibeh, B., Ma, J., Kobayashi, T., Quintero, A.J., and Huard, J. (2011). Follistatin improves skeletal muscle healing after injury and disease through an interaction with muscle regeneration, angiogenesis, and fibrosis. Am. J. Pathol. *179*, 915–930.

31. Lawlor, M.W., Read, B.P., Edelstein, R., Yang, N., Pierson, C.R., Stein, M.J., Wermer-Colan, A., Buj-Bello, A., Lachey, J.L., Seehra, J.S., and Beggs, A.H. (2011). Inhibition of activin receptor type IIB increases strength and lifespan in myotubularin-deficient mice. Am. J. Pathol. *178*, 784–793.

32. Qiao, C., Li, J., Jiang, J., Zhu, X., Wang, B., Li, J., and Xiao, X. (2008). Myostatin propeptide gene delivery by adeno-associated virus serotype 8 vectors enhances muscle growth and ameliorates dystrophic phenotypes in mdx mice. Hum. Gene Ther. *19*, 241–254.

33. Arounleut, P., Bialek, P., Liang, L.F., Upadhyay, S., Fulzele, S., Johnson, M., Elsalanty, M., Isales, C.M., and Hamrick, M.W. (2013). A myostatin inhibitor (propeptide-Fc) increases muscle mass and muscle fiber size in aged mice but does not increase bone density or bone strength. Exp. Gerontol. *48*, 898–904.

34. Zheng, H., Qiao, C., Tang, R., Li, J., Bulaklak, K., Huang, Z., Zhao, C., Dai, Y., Li, J., and Xiao, X. (2017). Follistatin N terminus differentially regulates muscle size and fat in vivo. Exp. Mol. Med. *49*, e377.

35. Lee, S.-J. (2007). Quadrupling muscle mass in mice by targeting TGF-β signaling pathways. PLoS ONE *2*, e789.

36. Poggioli, T., Vujic, A., Yang, P., Macias-Trevino, C., Uygur, A., Loffredo, F.S., Pancoast, J.R., Cho, M., Goldstein, J., Tandias, R.M., et al. (2016). Circulating growth differentiation factor 11/8 levels decline with age. Circ. Res. *118*, 29–37.

37. Yang, B., Larson, D.F., and Watson, R. (1999). Age-related left ventricular function in the mouse: analysis based on in vivo pressure-volume relationships. Am. J. Physiol. *277*, H1906–H1913.

38. Dai, D.-F., and Rabinovitch, P.S. (2009). Cardiac aging in mice and humans: the role of mitochondrial oxidative stress. Trends Cardiovasc. Med. *19*, 213–220.

39. Brack, A.S., and Rando, T.A. (2007). Intrinsic changes and extrinsic influences of myogenic stem cell function during aging. Stem Cell Rev. *3*, 226–237.

40. Gordon, K.J., and Blobe, G.C. (2008). Role of transforming growth factor-β superfamily signaling pathways in human disease. Biochim. Biophys. Acta *1782*, 197–228.

41. Mei, W., Xiang, G., Li, Y., Li, H., Xiang, L., Lu, J., Xiang, L., Dong, J., and Liu, M. (2016). GDF11 Protects against endothelial injury and reduces atherosclerotic lesion formation in apolipoprotein E-null mice. Mol. Ther. *24*, 1926–1938.

42. Rinaldi, F., Zhang, Y., Mondragon-Gonzalez, R., Harvey, J., and Perlingeiro, R.C.R. (2016). Treatment with rGDF11 does not improve the dystrophic muscle pathology of mdx mice. Skelet. Muscle *6*, 21.

43. Qiao, C., Li, J., Zheng, H., Bogan, J., Li, J., Yuan, Z., Zhang, C., Bogan, D., Kornegay, J., and Xiao, X. (2009). Hydrodynamic limb vein injection of adeno-associated virus serotype 8 vector carrying canine myostatin propeptide gene into normal dogs enhances muscle growth. Hum. Gene Ther. *20*, 1–10.

44. Xiao, X., Li, J., and Samulski, R.J. (1998). Production of high-titer recombinant adeno-associated virus vectors in the absence of helper adenovirus. J. Virol. *72*, 2224–2232.

45. Li, L., Yang, L., and Kotin, R.M. (2005). The DNA minor groove binding agents Hoechst 33258 and 33342 enhance recombinant adeno-associated virus (rAAV) transgene expression. J. Gene Med. *7*, 420–431.

YMTHE, Volume *26*

Supplemental Information

Neonatal Systemic AAV-Mediated Gene Delivery of GDF11 Inhibits Skeletal Muscle Growth

Quan Jin, Chunping Qiao, Jianbin Li, Juan Li, and Xiao Xiao

hGDF11

5′-

atggtgctggctgccccctgctgctgggatttctgctgctggctctggaactgcggcctagaggcgaagccgctga
aggaccagctgccgctgctgctgccgcagccgccgcagctgcagcaggcgtgggcggagaaagaagctctagacctg
cccctagcgtggcccctgagcctgatggatgtcctgtgtgcgtgtggcggcagcactccagagagctgcggctggaa
tccatcaagagccagatcctgagcaagctgagactgaaagaggcccccaacatcagccgcgaggtcgtgaaacagct
gctgcccaaagccccccccactgcagcagattctggacctgcacgacttccaggggacgccctgcagcccgaggatt
tcctggaagaggacgagtaccacgccaccaccgagacagtgatcagcatggcccaggaaaccgaccccgccgtgcag
acagatggcagccctctgtgctgccacttccacttcagccccaaagtgatgttcaccaaggtgctgaaagcccagct
gtgggtgtacctgaggcccgtgcctagaccagccaccgtgtacctgcagatcctgcggctgaagcctctgaccggcg
agggaacagctggcggcggaggggggaggaagaaggcacatcagaatcagaagcctgaagatcgagctgcacagcaga
agcggccactggcagagcatcgacttcaaacaggtgctgcactcctggttccggcagccccagagcaattggggcat
cgagatcaacgccttcgaccccagcggcaccgatctggccgtgacatctctgggacctggcgccgaaggcctgcacc
ccttcatggaactgagagtgctggaaaacaccaagcggagccggcggaacctgggcctggattgtgatgagcacagc
agcgagagccggtgctgcagataccccctgaccgtggacttcgaggcctttggctgggactggatcattgcccccaa
gcggtacaaggccaactactgcagcggccagtgcgagtacatgttcatgcagaagtacccccacacccacctggtgc
agcaggccaatcctagaggctctgccggcccttgctgcacccccacaaagatgagccccatcaacatgctgtacttc
aacgacaagcagcagatcatctacggcaagatccccggcatggtggtggacagatgcggctgctcc-3′

hGDF11Pro-Fc-1

5′-

gagctcaagcttaagctaacaaagaccacgacgatatcacggtcgtggtctcaaagaacaacaaacaacaaagtccg
actgagaaggagccaccatggtgctggctgctcctctgctgctgggattcctgctgctggccctggaactgaggcct
agaggcgaagccgctgaaggacctgctgccgctgccgcagccgccgctgcagcagcagctgcaggcgttggcggaga
gagatctagcagacctgccccttctgtggcccctgagcctgatggctgtcctgtgtgtgtgtggcggcagcacagca
gagagctgcggctggaatccatcaagagccagatcctgagcaagctgagactgaaagaggcccctaacatcagcaga
gaggtggtcaagcagctgctgcccaaggcccctccactgcagcagatcctggacctgcacgatttccagggcgacgc
tctgcagcccgaggacttcctggaagaggatgagtaccacgccaccaccgagacagtgatcagcatggcccaagaga
cagaccccgccgtgcagacagatggcagccctctgtgctgccacttccacttcagccccaaagtgatgttcaccaag
gtgctgaaggcccagctgtgggtgtacctgaggcctgtgcctagacccgccaccgtgtatctgcagatcctgcggct
gaagcctctgaccggcgagggaacagctggtggcggtggcggaggacggcggcacatcagaatcagaagcctgaaga
tcgagctgcactccagaagcggccactggcagagcatcgacttcaaacaggtgctgcacagctggttccggcagccc
cagagcaactggggcatcgagatcaacgccttcgaccccagcggcaccgatctggccgttacatctctgggacctgg
cgccgagggcctgcatccctttatggaactgcgggtgctggaaaacaccaaggacaagacccacacctgtcctccct
gccctgcccctgaactgctgggcggacctagcgtgttcctgttcccacccaagcccaaggacaccctgatgatcagc
cggacccctgaagtgacctgcgtggtggtggacgtgtcccacgaggatcccgaagtgaagttcaattggtacgtgga
cggcgtggaagtgcacaacgccaagaccaagcccagagaggaacagtacaacagcacctaccgggtggtgtccgtgc
tgaccgtgctgcaccaggactggctgaacggcaaagagtacaagtgcaaggtgtccaacaaggccctgcctgcccca
atcgagaaaaccatcagcaaggccaagggccagccccgcgagcctcaggtttacacactgcctcccagccgggaaga
gatgaccaagaaccaggtgtccctgacatgcctggtcaagggcttctaccccagcgatatcgccgtggaatgggaga
gcaacggccagcctgagaacaactacaagaccacccctcccgtgctggacagcgacggctcattcttcctgtacagc
aagctgaccgtggacaagagccggtggcagcagggcaacgtgttcagctgctctgtgatgcacgaggccctgcacaa
ccactacacccagaagtccctgtccctgagccccggcaagtgatgactcgaggcggccgc-3′

Supplemental Figure 1. Codon-optimized sequences for human GDF11 and human GDF11Pro-Fc-1.

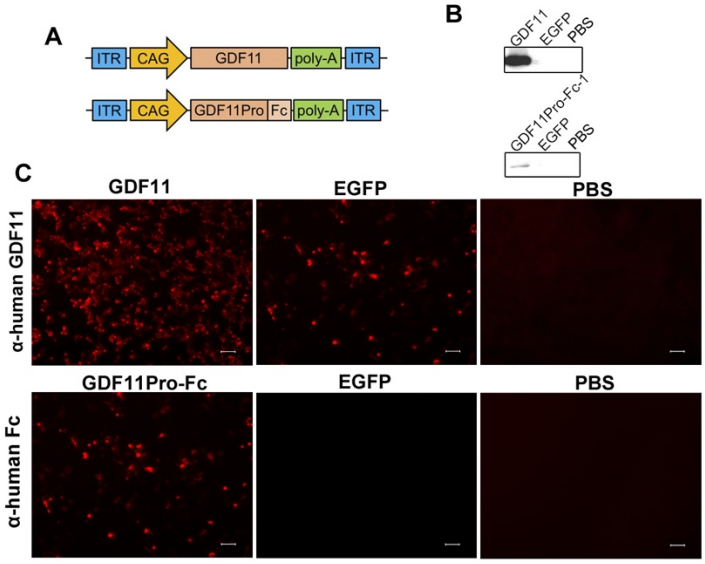

Supplemental Figure 2. (A) Vector construction. **(B)** Western blot analysis of cell lysates after vector reinfection with AAV9-GDF11 or AAV9-GDF11Pro-Fc-1 in HEK293 cells at a MOI of 10,000 vg/cell. AAV9-EGFP and PBS were used as control. **(C)** Representative immunofluorescence analysis confirmed the presence of the GDF11 and GDF11Pro-Fc-1 proteins after vector reinfection in HEK293 cells at a MOI of 10,000 vg/cell. 5 to 10 μM Hoechst 33342 was co-administered into HEK293 cells to facilitate transgene expression.

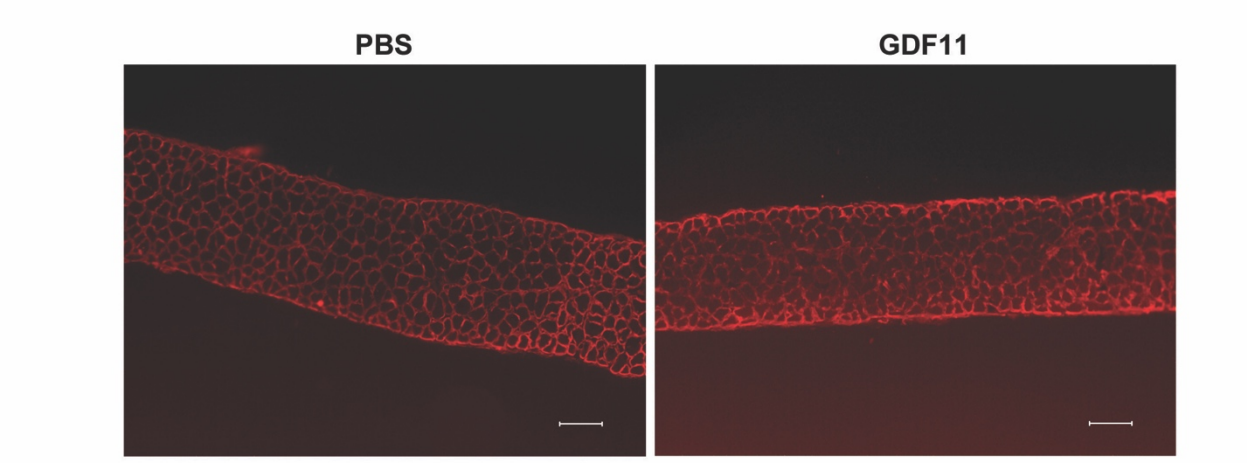

Supplemental Figure 3. Representative immunofluorescence sections from PBS-treated or AAV9-GDF11-treated diaphragm stained for laminin-α2 to visualize myofibers. Scale bar = 100 μm.

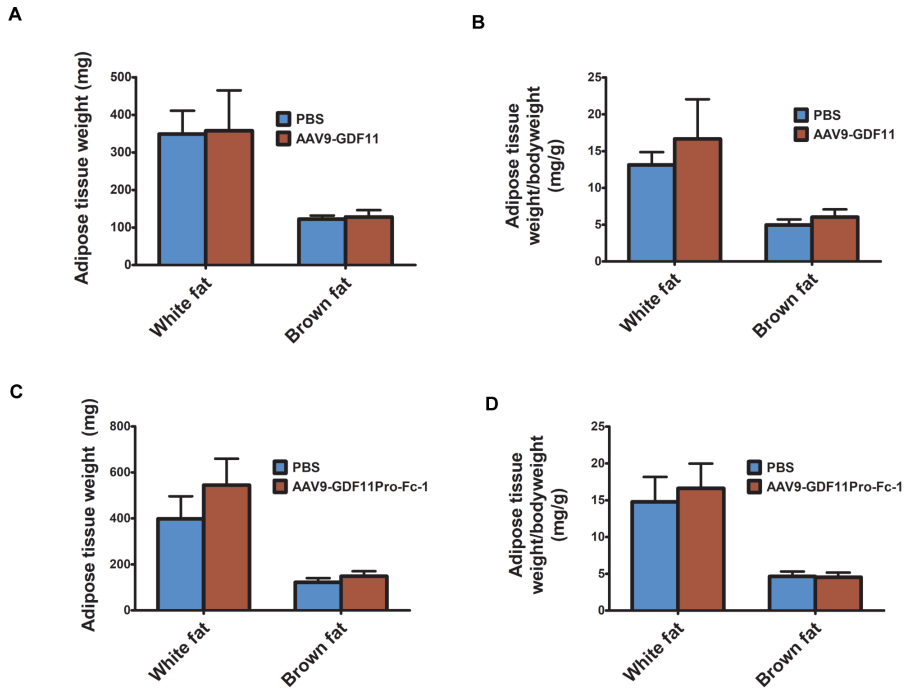

Supplemental Figure 4. Total and normalized mass of abdominal white fat depots and supraclavicular brown fat in mice treated with **(A,B)** AAV9-GDF11 or **(C,D)** AAV9-GDF11ProFc-1 compared to control.